

Decoupling Degradation and Content Processing for Adverse Weather Image Restoration

Xi Wang^{1,2*}, Xueyang Fu¹✉, Peng-Tao Jiang²✉, Jie Huang²,
Mi Zhou², Bo Li², Zheng-Jun Zha¹

¹ University of Science and Technology of China ² vivo Mobile Communication Co., Ltd

wangxxi@mail.ustc.edu.cn, xyfu@ustc.edu.cn, pt.jiang@vivo.com

Abstract

Adverse weather image restoration strives to recover clear images from those affected by various weather types, such as rain, haze, and snow. Each weather type calls for a tailored degradation removal approach due to its unique impact on images. Conversely, content reconstruction can employ a uniform approach, as the underlying image content remains consistent. Although previous techniques can handle multiple weather types within a single network, they neglect the crucial distinction between these two processes, limiting the quality of restored images.

This work introduces a novel adverse weather image restoration method, called DDCNet, which decouples the degradation removal and content reconstruction process at the feature level based on their channel statistics. Specifically, we exploit the unique advantages of the Fourier transform in both these two processes: (1) the degradation information is mainly located in the amplitude component of the Fourier domain, and (2) the Fourier domain contains global information. The former facilitates channel-dependent degradation removal operation, allowing the network to tailor responses to various adverse weather types; the latter, by integrating Fourier’s global properties into channel-independent content features, enhances network capacity for consistent global content reconstruction. We further augment the degradation removal process with a degradation mapping loss function. Extensive experiments demonstrate our method achieves state-of-the-art performance in multiple adverse weather removal benchmarks.

1. Introduction

Adverse weather conditions such as rain, haze, and snow commonly affect images, not only diminishing their visual

* : This work was done during the internship at vivo Mobile Communication Co., Ltd. Project was led by Peng-Tao Jiang.

✉ : Corresponding authors.

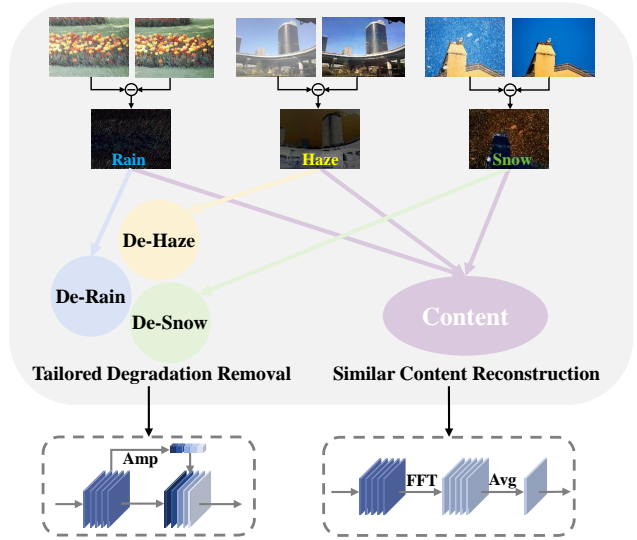


Figure 1. Adverse weather image restoration requires degradation removal and content reconstruction simultaneously. Different weather types necessitate tailored degradation removal due to their unique effects on images while the content reconstruction could be similar as the underlying image content remains consistent. In this paper, we decouple these two processes at the feature level based on their channel statistics and exploit the unique advantages of the Fourier transform to accomplish it.

quality but also hindering computer vision tasks like autonomous driving and object detection. To restore these adverse weather images, numerous algorithms have been developed over time. Initially, researchers employ handcraft-designed model priors [24, 52] to address various weather conditions. However, the inflexibility of these handcrafted model priors frequently resulted in less effective restoration outcomes, failing to adequately address the complexities of varying weather impacts. With the rapid advancement of deep learning, learning-based methods [10, 25, 33, 37] have exhibited remarkable abilities, many deep learning methods

have emerged for adverse weather restoration. Early approaches [3, 9, 13] focus on employing a single model to tackle one specific type of adverse weather condition. However, the performance of these networks is limited when faced with weather types they are not specifically designed for, limiting their usage flexibility. Hence, employing a single network to manage various adverse weather conditions is essential and holds substantial research importance.

Despite the growing number of methods [4, 23, 27, 34, 54] proposed to handle different degraded weather images using a unified framework, they all have certain shortcomings. All-in-One [23] introduces a network capable of restoring images under a variety of adverse weather conditions, however, its reliance on multiple encoders makes it computationally intensive. Transweather [34] integrates transformer architecture for the effective removal of severe weather effects, utilizing cross-attention and weather-type queries in the decoder for a comprehensive approach to adverse weather removal. However, it fits degradation information from the data, without considering the inherent degradation characteristics in the image itself. Zhu *et al.* [54] use a two-stage strategy, considering the general and specific characteristics of different adverse weather conditions separately. However, this model requires knowledge of weather types during inference, limiting its flexibility.

In fact, all previous methods have overlooked the necessity of separating the degradation removal and content reconstruction process for different weather types. Different weather types should be tailored for degradation removal due to their unique effects on images, while the content reconstruction can be similar as the underlying image content remains consistent for each weather type. Moreover, previous methods do not sufficiently mine the degradation information inherent in the image itself.

To address the above challenges, this paper introduces a novel approach, called DDCNet, to recover images of various adverse weather types in a unified network. As shown in Fig. 1, we decouple the degradation removal and the content reconstruction process into distinct modules at the feature level based on their channel statistics. Due to the variation in channel distribution among different degradation types, we modulate the features along the channel dimension to achieve channel-dependence degradation removal. Moreover, recognizing the crucial role of global information in content reconstruction, we employ it to facilitate the attainment of consistent image reconstruction. Owing to the rich information brought by the Fourier transform, we utilize it to assist these two processes. Specifically, in the degradation removal module, we utilize the amplitude of the Fourier domain, which primarily contains image degradation information, extracting channel-dependence degradation information to adjust the importance between channels. This allows the network to generate tailored responses for various

degradations. In the content reconstruction module, we extract the channel-independence content feature and utilize the global characteristics of Fourier space, allowing the network to process the background content of any weather condition in a consistent and global manner. Additionally, we integrate a degradation mapping loss function to constrain the direction of degradation removal.

The contributions of this paper could be summarized as:

- This research first highlights the tailored degradation removal and similar content reconstruction processes for various adverse weather types. By decoupling these two processes based on their channel statistics, it reduces the complexity of the unified network in handling multiple adverse weather types.
- We propose a new method for channel-dependent degradation removal by utilizing the degradation-related amplitude part in the Fourier space as an auxiliary component. Furthermore, we utilize Fourier’s global properties to bolster channel-independent globally consistent content reconstruction, enhancing the restoration of weather-impacted images.
- The proposed method can restore images of different weather types in a unified network. We conduct extensive experiments on several adverse weather removal benchmarks and outperform previous multi-task state-of-the-art methods.

2. Related Works

Adverse weather removal, such as draining [9, 15, 36], raindrop removal [28, 31, 49], dehazing [13, 33, 44], and desnowing [3, 25, 50], has gained attention in recent years, and we summarize them as follows.

Single Image Deraining. Currently, single image deraining primarily uses CNN-based methods. Fu *et al.* [9] introduced global residual learning into single image deraining and demonstrated the effectiveness of a deeper structure in rain streak removal. Subsequently, numerous CNN-based rain streak removal methods [2, 5, 18, 22, 37, 43, 46, 51, 53], were proposed, and raindrop removal [12, 28, 30, 31, 49], which differs from rain streak removal, was also introduced. In order to better restore texture details and improve visual quality, Zhang *et al.* [48] utilized GANs to handle rain raindrops. IDT [40] combines the advantages of transformers and CNNs, uses non-local information and retains high-frequency components, achieving better results in rain image restoration.

Single Image Dehazing. He *et al.* [13] utilize dark channel prior for Single image haze removal. Subsequently, some methods used CNNs to estimate the parameters of degraded haze images. Some methods [1, 13, 29, 33, 41, 44]

also directly use an end-to-end learning approach to map haze images directly to clean images. Some work is also dedicated to the restoration of real-world haze images, and it is combined with unsupervised methods.

Single Image Desnowing. DesnowNet [25] uses a two-stage network learning approach for snow removal. To cope with the challenges posed by snow of multiple sizes and non-transparency, Chen *et al.* [3] proposed a unified approach dealing with size and transparency concurrently, it also achieved the removal of both snow and haze.

All-in-One Adverse Weather Removal. Different from the removal of a single adverse weather condition, for practicality, an increasing number of studies are focusing on handling multiple weather deteriorations using a single network. Li *et al.* [23] use task-specific encoders for each type of adverse weather and use a neural architecture search to optimize the processing of image features extracted from all encoders, thus achieving all-in-one image restoration. For the first time, TransWeather [34] introduces the transformer into all-in-one adverse weather restoration. It leverages the attention mechanism in the transformer and sets the query in the decoder as adaptively learned parameters to realize adaptive processing for different weather conditions. Chen *et al.* [4] employ a two-stage training strategy, by distilling the knowledge learned from multiple "teacher" networks responsible for different weather conditions in the first stage to the "student" network in the second stage, thus achieving promising results in various bad weather removal tasks. With the popularity of generative models, WeatherDiffusion [27] first introduces the diffusion model into adverse weather removal, its patch-based methodology enables the model to recover images of any size while maintaining quality. Zhu *et al.* [54] also adopt a two-stage learning strategy, by adaptively adding parameters for different weather types in the second stage to handle various weather conditions. However, these methods require the introduction of additional network structures or need to know the weather type during inference. Our method considers unique degradation removal and similar content reconstruction for different adverse weather conditions, reducing the complexity of the unified network in handling multiple adverse weather types. Furthermore, we achieve blind weather image restoration by exploiting the inherent degradation information present in the image itself.

3. Method

In this chapter, we start by discussing the necessity of separately handling degradation removal and content reconstruction processes, outlining the motivation behind our proposal. Following this, we detail how to effectively sepa-

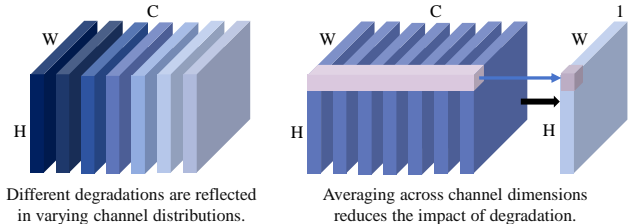


Figure 2. Channel statistics for degradation removal and content reconstruction decoupling.

rate these processes and explain the use of the Fourier transform as an auxiliary to assist these processes. Additionally, we introduce the degradation mapping loss function proposed in our approach.

3.1. Background and Motivation

Adverse weather image restoration seeks to recover clear images from those affected by various weather conditions (e.g., rain, haze, and snow). Different weather conditions call for specific processes for degradation removal because they affect images in unique ways. Yet, content reconstruction can follow a single process since the underlying content of the image remains the same. Therefore, separating the processes of degradation removal and content reconstruction can reduce the complexity faced by a single model in handling multiple types of adverse weather conditions. While previous techniques address multiple weather conditions within a single network, they have neglected the importance of using specific attributes for these two processes, consequently resulting in sub-optimal results.

In this paper, we decouple the degradation removal and content reconstruction based on their channel statistics, which is shown in Fig. 2. For degradation removal, we adjust the features along the channel dimension based on the differences in degradation distribution across different weather conditions. For content reconstruction, the content exists in a channel-independent space, and global information plays a vital role. Therefore, we use channel-dependent degradation guidance information and channel-independent global content information to implement these two processes respectively. To achieve this, we utilize the unique advantages of Fourier to assist these two processes: (1) the degradation information of images is primarily concentrated in the amplitude, and (2) Fourier has the capability to capture global information. Therefore, in the degradation removal module (DRM), we utilize the amplitude to generate distinctive conditional information to guide the network to generate different responses for various types of weather. In the content reconstruction module (CRM), we leverage the global information capture property of Fourier to achieve global content reconstruction. Additionally, since there are discernible differences in the optimization direc-

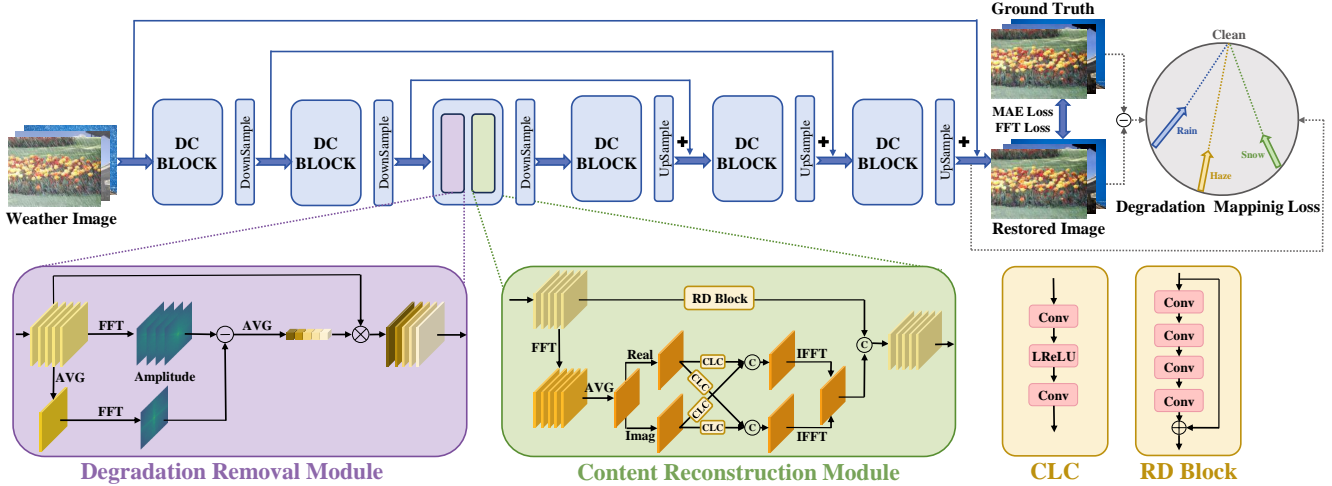


Figure 3. The overall of our proposed UDCNet framework, which manages the degradation removal and content reconstruction in separate modules based on their channel statistics. Specifically, to achieve tailored channel-dependent degradation removal, we utilize the degradation-related amplitude part in the Fourier domain to modulate the feature along the channel dimension. For channel-independent content reconstruction, we average the feature along the channel to eliminate degradation information and use Fourier’s global properties to accomplish globally consistent content reconstruction. Additionally, we introduce a novel degradation mapping loss function, utilizing degraded images to strengthen the degradation removal process.

tions among various adverse weather conditions, which primarily concentrate on the degradation information, we have further proposed a degradation mapping loss function to constrain their optimization direction. In this way, the network reduces the difficulty of multiple degradation processing, thereby achieving high-quality restoration results.

3.2. The Network Framework

Our objective is to recover clean background contents from images damaged by various adverse weather conditions. To achieve our goal, we propose a novel unified framework, called DDCNet. Our framework utilizes a multi-scale U-Net architecture that incorporates three encoders and three decoders. Each encoder and decoder mainly consists of two components: the degradation removal module and the content reconstruction module. This setup includes three upsampling and downsampling operations. The input and output dimensions of each module remain consistent. Our detailed framework is shown in Fig. 3. In the following, we will introduce these two important modules in detail.

Degradation Removal Module (DRM) In the degradation removal module, as the distribution of different degradations varies across channels, the goal of this module is to modulate feature channels according to the degradation. To achieve this, we leverage the observation that degradation information in an image is mainly concentrated in the amplitude part of the Fourier domain. By utilizing the amplitude’s characteristics, we generate channel-dependent

degradation conditional information, enabling the network to focus more on removing adverse weather degradation.

Formally, let $\mathbf{X} \in \mathbb{R}^{H \times W \times C}$ denote the input feature of DRM. When inputting \mathbf{X} to DRM, we first apply the Fourier transform to it in terms of spatial dimensions, which can be expressed as:

$$\hat{\mathbf{X}}_{u,v} = \frac{1}{\sqrt{HW}} \sum_{h=0}^{H-1} \sum_{w=0}^{W-1} \mathbf{X}_{h,w} \times e^{-j2\pi(\frac{h}{H}u + \frac{w}{W}v)}, \quad (1)$$

where u, v denotes the coordinates of the Fourier space feature $\hat{\mathbf{X}}$. Then we can generate the amplitude component \mathbf{A} by:

$$\mathbf{A} = \sqrt{\mathbf{R}^2 + \mathbf{I}^2}, \quad (2)$$

where \mathbf{R} and \mathbf{I} are real and imaginary parts of $\hat{\mathbf{X}}$, respectively. The amplitude \mathbf{A} contains both channel-dependent and channel-independent degradation information, but we only need channel-dependent degradation information to modulate feature channels for various weather conditions. Thus, to generate the channel-dependent degradation information from \mathbf{A}_{deg} , we further generate the channel-independent degradation information and remove it from \mathbf{A} . Specifically, we first average the input features \mathbf{X} across the channel dimension and generate the channel-independent feature $\mathbf{X}_{ci} \in \mathbb{R}^{H \times W \times 1}$. Then, we perform a Fourier transform to \mathbf{X}_{ci} and generate its amplitude \mathbf{A}_{ci} , where \mathbf{A}_{ci} contains channel-independent degradation information. To extract the differences in degradations across channels, we remove \mathbf{A}_{ci} from \mathbf{A} :

$$\mathbf{A}_{deg} = \mathbf{A} - \mathbf{A}_{ci}. \quad (3)$$

By the above operations, we can obtain the channel-dependent degradation information \mathbf{A}_{deg} . After that, we transform \mathbf{A}_{deg} to channel-dependent degradation condition $\mathbf{v}_{con} \in \mathbb{R}^{1 \times 1 \times C}$ by a project network consisting of a global average pooling layer, two consecutive linear layers and a sigmoid function, which is formulated as

$$\mathbf{S}_{con} = \text{Sigmoid}(f_{p2}(\text{ReLU}(f_{p1}(\mathbf{v}_{con})))), \quad (4)$$

where f_{p1} and f_{p2} denote the linear layers. The condition vector \mathbf{S}_{con} modulates the original features \mathbf{X} , directing the network involves combining channel information based on important relationships to perform degradation removal operations. Consequently, the modulated degradation removal feature $\mathbf{X}_d \in \mathbb{R}^{H \times W \times C}$ is generated by

$$\mathbf{X}_d = \mathbf{X} \cdot \mathbf{S}_{con}, \quad (5)$$

where \mathbf{S}_{con} is broadcast to the shape of \mathbf{X} for a dot product.

Content Reconstruction Module (CRM) For content reconstruction, both local and global content information plays crucial roles. Therefore, in this module, we utilize two branches, one for local detail captured and the other for global content captured.

In the global branch, we pursue processing global content information that is independent of degradation. Leveraging the power of the Fourier transform to capture global information, our approach begins by converting the degradation removal feature \mathbf{X}_{deg} into the Fourier domain as $\hat{\mathbf{X}}_{deg}$. This transformation enables us to encode the spatial-global information of the feature. Subsequently, drawing inspiration from [20], we employ channel dimension averaging of features to minimize the presence of degradation information. By averaging $\hat{\mathbf{X}}_{deg}$ along the channel dimension, we obtain a single-channel feature denoted as $\hat{\mathbf{X}}_s \in \mathbb{R}^{H \times W \times 1}$, which represents channel-independent global content information. Therefore, our model can effectively extract essential information for content reconstruction. Moving forward, we extract the real part, $\hat{\mathbf{X}}_{real}$, and the imaginary part, $\hat{\mathbf{X}}_{imag}$, from the transformed feature $\hat{\mathbf{X}}_s$. Finally, we synergistically combine the extracted features from the real and imaginary branches. This integration is accomplished through an interplay of feature interactions, which is formulated as follows:

$$\begin{aligned} \mathbf{X}_{real} &= f_1([f_{clc,11}(\mathbf{X}_{real}), f_{clc,12}(\mathbf{X}_{imag})]), \\ \hat{\mathbf{X}}_{imag} &= f_2([f_{clc,21}(\mathbf{X}_{real}), f_{clc,22}(\mathbf{X}_{imag})]), \end{aligned} \quad (6)$$

where $[,]$ represents the concatenation operation, f_1 and f_2 both indicate a 3×3 convolution. $f_{clc,*}$ indicates a CLC block including two 3×3 convolutions with a LeakyReLU activation function in between. Then, we transform the features to the original space $\mathbf{X}_{tem} \in \mathbb{R}^{H \times W \times C}$ by performing IFFT transformations on $\hat{\mathbf{X}}_{real}$ and $\hat{\mathbf{X}}_{imag}$.

In the global branch, taking the average over the channel dimension inevitably results in some content detail loss. Therefore, in the local branch, we introduce a residual dense block (RDB) consisting of convolutional layers to capture local detailed features. The RDB helps preserve information and enhance feature representation. The input of the RDB is \mathbf{X}_{deg} and the output of the RDB is denoted as $\mathbf{X}_r \in \mathbb{R}^{H \times W \times C}$. Finally, to aggregate global and local information, we concatenate \mathbf{X}_{tmp} and \mathbf{X}_r toward the channel dimension. The concatenated result is then passed through a 1×1 convolution. The final output of this operation is referred to as $\mathbf{X}_{con} \in \mathbb{R}^{H \times W \times C}$.

3.3. Loss Function

In this paper, we employ three loss functions to optimize our model, in which the proposed degradation mapping loss is specifically designed for handling multiple adverse weather conditions. Let \mathbf{I}_{in} denote the input adverse weather image, \mathbf{I}_{out} denote the network's output image, and \mathbf{I}_{gt} denote the corresponding ground truth.

Degradation Mapping Loss (DM). We constrain the network optimization process by incorporating weather type into the loss function. Specifically, we first compute the residual between the input image and the network's output image, as well as the residual between the input image and the ground truth, then maximize the cosine similarity between these residuals to enforce consistency in the direction of degradation removal, which is formulated as:

$$L_{DA}(\mathbf{I}_{in}, \mathbf{I}_{out}, \mathbf{I}_{gt}) = 1 - \langle \mathbf{I}_{out} - \mathbf{I}_{in}, \mathbf{I}_{gt} - \mathbf{I}_{in} \rangle, \quad (7)$$

where $\langle \cdot, \cdot \rangle$ represents the cosine similarity.

Mean Absolute Error Loss (MAE). Since MAE is insensitive to outliers and has better robustness than mean squared error (MSE) for better edges and textures restoration, we choose MAE to train our network:

$$L_{MAE}(\mathbf{I}_{out}, \mathbf{I}_{gt}) = \|\mathbf{I}_{gt} - \mathbf{I}_{out}\|_1. \quad (8)$$

FFT Loss. Since the frequency domain distribution of degraded images differs from that of clean compartments, we also impose the constraint in the frequency domain. Specifically, we first conduct the Fast Fourier Transform (FFT) of the resorted image and ground truth, then measure the mean absolute error between them, which is formulated as:

$$L_{FFT}(\mathbf{I}_{out}, \mathbf{I}_{gt}) = \|\text{FFT}(\mathbf{I}_{gt}) - \text{FFT}(\mathbf{I}_{out})\|_1, \quad (9)$$

where FFT stands for fast Fourier transform, which converts an image to the frequency domain. Therefore, the overall loss function can be formulated as:

$$L_{TOTAL} = \lambda_1 L_{MAE} + \lambda_2 L_{FFT} + \lambda_3 L_{DM}. \quad (10)$$

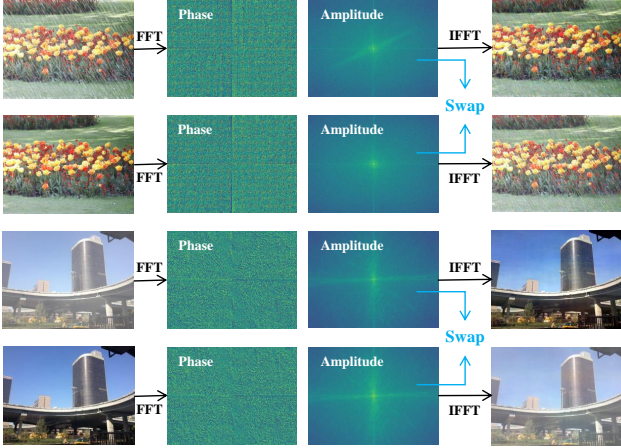


Figure 4. We swap the amplitude of the adverse weather image with its clean compartment, as can be seen, the attributes of ‘degradation’ and ‘clean’ are transferred along with the amplitude.

3.4. Discussion

To further understand the rationality of using Fourier transforms for degradation removal and content reconstruction process, we conduct some visual analysis as demonstrated in Fig. 4 and Fig. 5.

As empirically verified in [16], the degradation information in a weather image is mainly concentrated in the amplitude part of the Fourier domain. As shown in Fig. 4, when we swap the amplitude of the image with adverse weather conditions and its corresponding ground truth, we can see that the attributes of ‘degradation’ and ‘clean’ are transferred along with the amplitude. This validates our approach of utilizing amplitude to generate the degradation condition information.

Furthermore, as shown in Fig. 5, the corresponding visualizations distinctly demonstrate how degradation is differently addressed for various weather patterns. For instance, images degraded by snow integrate higher frequency components due to snow particles. The snow removal process aligns these images closer to the lower frequencies seen in ground truth images. In contrast, haze removal increases the frequency details, as hazy images have lower frequency contents compared to their sharper ground truths. Therefore, we propose a degradation mapping loss to constrain the direction of degradation removal to align with the ‘clean’ direction, thus further strengthening the degradation removal process.

For content reconstruction, As shown in Eqn.1, each pixel in the Fourier space interacts with all the pixels in the spatial domain. We utilize this characteristic of Fourier to achieve global content reconstruction, which complements the local detail reconstruction.

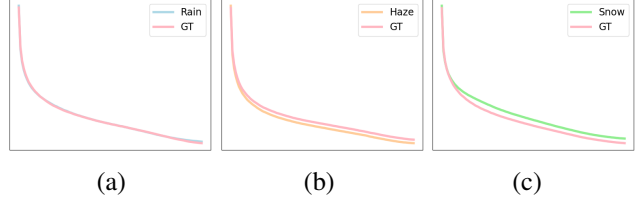


Figure 5. We randomly select 500 images from each adverse weather dataset in [Setting2], and plot the amplitude statistics of these images, labeled as (a), (b), and (c) for rain, haze, and snow, respectively. These graphs distinctly illustrate that different adverse weather types exhibit unique optimization directions in their frequency amplitude.

Table 1. Quantitative results on the [Setting1] test dataset. PSNR / SSIM format. The best results are **boldfaced**.

Type	Method	Outdoor-Rain		RainDrop	
		PSNR \uparrow	SSIM \uparrow	PSNR \uparrow	SSIM \uparrow
Single-Task	pix2pix [17]	19.09	0.71	28.02	0.85
	HRGAN [21]	21.56	0.86	-	-
	Attn.Gan [28]	-	-	30.55	0.90
	MPRNet [47]	21.90	0.85	-	-
	CCN [30]	-	-	31.34	0.95
Multi-Tasks	All-in-One [23]	24.71	0.90	31.12	0.93
	TransWeather [34]	23.18	0.84	28.98	0.90
	Chen <i>et al.</i> [4]	23.94	0.85	30.75	0.91
	Zhu <i>et al.</i> [54]	25.31	0.90	31.31	0.93
	Ours	25.59	0.90	31.69	0.93

Table 2. Quantitative results on the SnowTest100k-L test dataset. PSNR / SSIM format. The best results are **boldfaced**.

Type	Method	Setting1		Setting2	
		PSNR \uparrow	SSIM \uparrow	PSNR \uparrow	SSIM \uparrow
De-Snow	DetailsNet [6]	19.18	0.75	19.18	0.75
	DesnowNet [25]	27.17	0.90	27.17	0.90
	JSTASR [3]	25.32	0.81	25.32	0.81
	DDMSNET [50]	28.85	0.88	28.85	0.88
Multi-Tasks	All-in-one [23]	28.33	0.88	-	-
	Transformer [34]	27.80	0.85	26.17	0.88
	Chen <i>et al.</i> [4]	29.27	0.88	28.71	0.88
	Zhu <i>et al.</i> [54]	29.71	0.89	29.42	0.89
	Ours	30.59	0.91	30.45	0.90

4. Experiments

This section introduces our experimental setup and compares our performance with other techniques.

4.1. Experimental Settings

Datasets. To verify the effectiveness of our network framework, we employed two experimental dataset settings.

[Setting 1] includes three different adverse weather datasets: ‘Raindrop’ [28], ‘Outdoor-Rain’ [22], and ‘Snow100K’ [25]. ‘Raindrop’ consists of 861 paired training images and two test sets, Test A and Test B, which contain 58 and 249 paired images respectively. ‘Outdoor-Rain’ comprises 9,000 paired training images and 1,500 paired

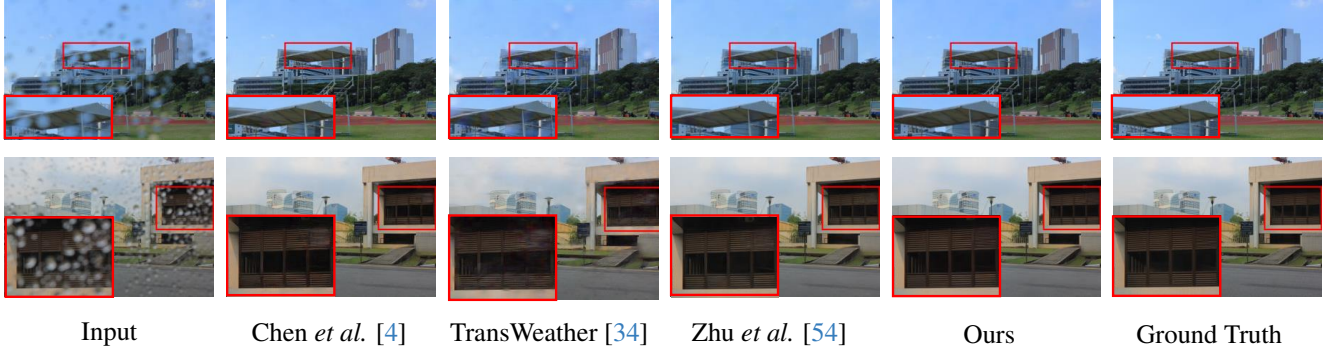


Figure 6. Visual comparison of image deraining on the RainDrop dataset. Zoom in for better comparison.

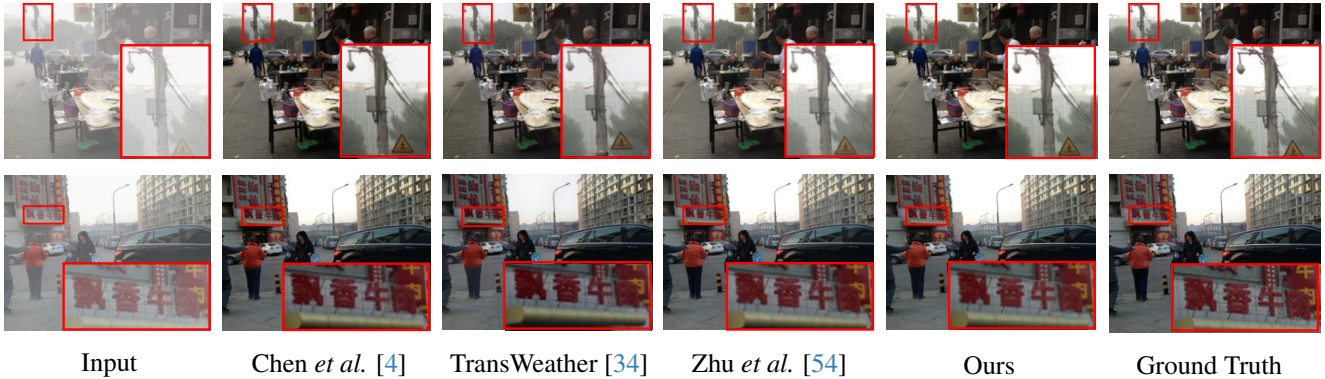


Figure 7. Visual comparison of image dehaizing on the RESIDE dataset. Zoom in for better comparison.

Table 3. Quantitative results on the [Setting2] test dataset. PSNR / SSIM format. The best results are **boldfaced**.

Type	Rain14K			RESIDE		
	Method	PSNR \uparrow	SSIM \uparrow	Method	PSNR \uparrow	SSIM \uparrow
Single-Task	JORDER [42]	31.28	0.92	EPDN [29]	23.82	0.89
	PReNet [32]	31.88	0.93	PFDN [8]	31.45	0.97
	DRD-Net [6]	29.65	0.88	KDDN [14]	33.49	0.97
	MSPFN [7]	29.24	0.88	MSBDN [7]	33.79	0.98
	DualGCN [11]	30.50	0.91	FFA-Net [26]	34.98	0.99
	JRJG [45]	31.18	0.91	AECRNet [39]	35.61	0.98
	MPRNet [47]	31.53	0.96	MPRNet [47]	31.31	0.97
Multi-Tasks	All-in-One [23]	30.82	0.90	All-in-One [23]	30.49	0.95
	TransWeather [34]	29.14	0.89	TransWeather [34]	27.66	0.95
	Chen et al. [4]	31.75	0.91	Chen et al. [4]	30.76	0.97
	Zhu et al. [54]	32.49	0.93	Zhu et al. [54]	30.85	0.98
	Ours	32.57	0.93	Ours	31.62	0.98

testing images. ‘Snow100K’ encompasses 50K paired training images and three test datasets: ‘Snow100K-S’, ‘Snow100K-M’, and ‘Snow100K-L’, which contain 16,611, 16,588, and 16,801 paired images respectively.

[Setting 2] also includes datasets of three different types of severe weather: ‘Rain14K’ [10], ‘RESIDE’, and ‘Snow100K’ [25], with the latter being the same as in Setting 1. ‘Rain14K’ comprises 12,600 paired training images and 1,400 paired test images. ‘RESIDE’ includes 313,944 paired training images and two test sets, ‘SOTS-Test-outdoor’ and ‘SOTS-Test-indoor’, each containing 500

paired images. To ensure fairness in comparisons, we employ the method described in [34, 54] to uniformly sample images from the dataset during network training.

Implementation details. We conducted our experiments on four NVIDIA GTX 4090 GPUs. Each training iteration involves randomly shuffling images with a batch size of 32. Images are cropped to patches of size 224×224 . Our network is trained for 300 epochs with the Adam optimization algorithm [19]. The learning rate starts at $2e-4$ and decays by cosine annealing scheme until $1e-6$.

4.2. Comparison with State-of-the-Art Methods

To assess the performance of our network, we employed well-established evaluation metrics, including peak signal-to-noise ratio (PSNR) and structural similarity index (SSIM) [38]. These metrics are utilized as quantitative measures to evaluate the effectiveness of our network.

We present our quantitative results in Tab. 1, Tab. 2, and Tab. 3, including both all-weather-removal and typical-weather-removal methods. As can be seen from the tables, compared with all-weather-removal methods, our method achieved state-of-the-art performance across all synthetic test sets. We will present additional visualizations in the supplementary materials. Furthermore, we demonstrate the visual effects of our approach in the Fig. 6 and Fig. 7, which

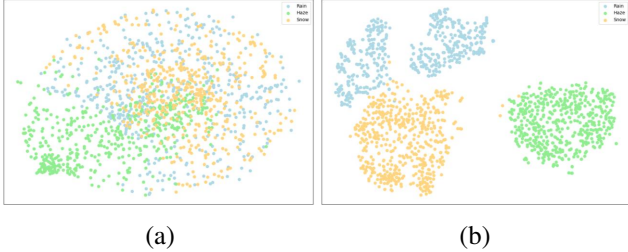


Figure 8. The t-SNE [35] visualization of the features from the last encoder block: (a) illustrates the input features of this block, and (b) depicts their amplitudes.

show that our method restores texture details more effectively, further illustrating the efficacy of our approach. Due to space constraints, we will present additional visual effect analysis in the supplementary materials.

4.3. Ablation Studies

We conducted ablation experiments on the [Setting 2] Rain14K dataset to verify the effectiveness of our method.

Investigation of the DRM. To demonstrate the effectiveness of amplitude information from Fourier transforms in guiding the degeneration removal process, we omitted the amplitude guidance (AG) step from all degeneration removal modules in the network. This modified model is henceforth referred to as ‘Model-1.’ As shown in Tab. 4, quantitative analysis confirms the usefulness of amplitude as a guide for degeneration removal. To further validate the effectiveness of extracting channel-independence degradation information, we removed the step involving subtraction of the norm amplitude (SNA) from the features, resulting in a variation named ‘Model-2.’ The quantitative results support the efficacy of this operation.

To more vividly demonstrate the rationale behind using amplitude as guidance information, we performed t-SNE [35] visualization analysis on the features from the last encoder block. Fig. 8(a) represents the input features of this block, while Fig. 8(b) depicts their amplitudes. It is apparent that the amplitude can significantly distinguish different adverse weather types.

Investigation of the CRM. To demonstrate the efficacy of our proposed content restructuring module, we replaced all instances of this module within the network with convolutionally stacked RD Blocks, resulting in a modified architecture we refer to as ‘Model-3.’ Quantitative results, presented in Tab. 4, indicate that our specifically designed module achieved superior performance.

Investigation of the Loss Function We also investigated the effect of different loss function combinations on network performance. We set λ_2 and λ_3 to 0 respectively to

Table 4. Ablation study of our training strategy using the PSNR metric on the Rain14K of [Setting 2]. **AG**: omit the amplitude guidance step. **SNA**: remove subtraction of the norm amplitude. **CR**: replaced all content reconstruction modules with RD Blocks.

Method	AG	SNA	CR	PSNR / SSIM
Model-1			✓	32.24 / 0.93
Model-2	✓		✓	32.42 / 0.93
Model-3	✓	✓		32.39 / 0.93
Ours	✓	✓	✓	32.57 / 0.93

Table 5. Quantitative results(PSNR) of different loss function combinations.

No.	λ_1	λ_2	λ_3	PSNR
1	1	1	0	32.37
2	1	0	1	32.34
3	1	1	1	32.57

Table 6. The comparison between our method and other methods in terms of parameter and PSNR shows that our method has achieved the best overall performance.

Methods	All-in-One	TransWeather	Chen <i>et al.</i>	Ours
#Param (M)	44.0	38.1	28.7	11.2
PSNR(dB)	30.82	29.14	31.75	32.57

validate the effectiveness of these two loss functions. The quantitative results are shown in Tab. 5, indicating that both loss functions contribute to performance improvement.

Parameter comparisons. We present a comparison of our method with others in terms of parameters and performance in Tab. 6, and it can be seen that our method achieves better performance with fewer parameters.

5. Conclusion

In this paper, we first identify the distinctions in degradation removal and content reconstruction processes for different adverse weather conditions. Then we decouple these two processes into distinct modules based on their channel statistics. The degradation removal module utilizes the observation that degradation information in images primarily concentrates on the Fourier domain’s amplitude, generating channel-dependence degradation condition information to modulate the features along the channel dimension. This allows unique responses to different adverse weather types. The content reconstruction module mitigates the influence of degradation information by taking the mean of features along the channel dimension. Additionally, it exploits the global properties of the Fourier transform to enable consistent global content reconstruction. Our framework reduces the challenges of handling various adverse weather types in a unified network, thereby enhancing its performance. The effectiveness of our method is demonstrated in various weather conditions.

References

- [1] Bolun Cai, Xiangmin Xu, Kui Jia, Chunmei Qing, and Dacheng Tao. Dehazenet: An end-to-end system for single image haze removal. *IEEE transactions on image processing*, 25(11):5187–5198, 2016. 2
- [2] Chenghao Chen and Hao Li. Robust representation learning with feedback for single image deraining. In *Proceedings of the IEEE/CVF conference on computer vision and pattern recognition*, pages 7742–7751, 2021. 2
- [3] Wei-Ting Chen, Hao-Yu Fang, Jian-Jiun Ding, Cheng-Che Tsai, and Sy-Yen Kuo. Jstasr: Joint size and transparency-aware snow removal algorithm based on modified partial convolution and veiling effect removal. In *Computer Vision–ECCV 2020: 16th European Conference, Glasgow, UK, August 23–28, 2020, Proceedings, Part XXI 16*, pages 754–770. Springer, 2020. 2, 3, 6
- [4] Wei-Ting Chen, Zhi-Kai Huang, Cheng-Che Tsai, Hao-Hsiang Yang, Jian-Jiun Ding, and Sy-Yen Kuo. Learning multiple adverse weather removal via two-stage knowledge learning and multi-contrastive regularization: Toward a unified model. In *Proceedings of the IEEE/CVF Conference on Computer Vision and Pattern Recognition*, pages 17653–17662, 2022. 2, 3, 6, 7, 4
- [5] Xiang Chen, Jinshan Pan, Kui Jiang, Yufeng Li, Yufeng Huang, Caihua Kong, Longgang Dai, and Zhentao Fan. Unpaired deep image deraining using dual contrastive learning. In *Proceedings of the IEEE/CVF Conference on Computer Vision and Pattern Recognition*, pages 2017–2026, 2022. 2
- [6] Sen Deng, Mingqiang Wei, Jun Wang, Yidan Feng, Luming Liang, Haoran Xie, Fu Lee Wang, and Meng Wang. Detail-recovery image deraining via context aggregation networks. In *Proceedings of the IEEE/CVF conference on computer vision and pattern recognition*, pages 14560–14569, 2020. 6, 7
- [7] Hang Dong, Jinshan Pan, Lei Xiang, Zhe Hu, Xinyi Zhang, Fei Wang, and Ming-Hsuan Yang. Multi-scale boosted dehazing network with dense feature fusion. In *Proceedings of the IEEE/CVF conference on computer vision and pattern recognition*, pages 2157–2167, 2020. 7
- [8] Jiangxin Dong and Jinshan Pan. Physics-based feature dehazing networks. In *Computer Vision–ECCV 2020: 16th European Conference, Glasgow, UK, August 23–28, 2020, Proceedings, Part XXX 16*, pages 188–204. Springer, 2020. 7
- [9] Xueyang Fu, Jiabin Huang, Xinghao Ding, Yinghao Liao, and John Paisley. Clearing the skies: A deep network architecture for single-image rain removal. *IEEE Transactions on Image Processing*, 26(6):2944–2956, 2017. 2
- [10] Xueyang Fu, Jiabin Huang, Delu Zeng, Yue Huang, Xinghao Ding, and John Paisley. Removing rain from single images via a deep detail network. In *Proceedings of the IEEE conference on computer vision and pattern recognition*, pages 3855–3863, 2017. 1, 7
- [11] Xueyang Fu, Qi Qi, Zheng-Jun Zha, Yurui Zhu, and Xinghao Ding. Rain streak removal via dual graph convolutional network. In *Proceedings of the AAAI Conference on Artificial Intelligence*, pages 1352–1360, 2021. 7
- [12] Zhixiang Hao, Shaodi You, Yu Li, Kunming Li, and Feng Lu. Learning from synthetic photorealistic raindrop for single image raindrop removal. In *Proceedings of the IEEE/CVF International Conference on Computer Vision Workshops*, pages 0–0, 2019. 2
- [13] Kaiming He, Jian Sun, and Xiaoou Tang. Single image haze removal using dark channel prior. *IEEE transactions on pattern analysis and machine intelligence*, 33(12):2341–2353, 2010. 2
- [14] Ming Hong, Yuan Xie, Cuihua Li, and Yanyun Qu. Distilling image dehazing with heterogeneous task imitation. In *Proceedings of the IEEE/CVF Conference on Computer Vision and Pattern Recognition*, pages 3462–3471, 2020. 7
- [15] Xiaowei Hu, Chi-Wing Fu, Lei Zhu, and Pheng-Ann Heng. Depth-attentional features for single-image rain removal. In *Proceedings of the IEEE/CVF Conference on computer vision and pattern recognition*, pages 8022–8031, 2019. 2
- [16] Jie Huang, Yajing Liu, Feng Zhao, Keyu Yan, Jinghao Zhang, Yukun Huang, Man Zhou, and Zhiwei Xiong. Deep fourier-based exposure correction network with spatial-frequency interaction. In *European Conference on Computer Vision*, pages 163–180. Springer, 2022. 6
- [17] Phillip Isola, Jun-Yan Zhu, Tinghui Zhou, and Alexei A Efros. Image-to-image translation with conditional adversarial networks. In *Proceedings of the IEEE conference on computer vision and pattern recognition*, pages 1125–1134, 2017. 6
- [18] Kui Jiang, Zhongyuan Wang, Peng Yi, Chen Chen, Baojin Huang, Yimin Luo, Jiayi Ma, and Junjun Jiang. Multi-scale progressive fusion network for single image deraining. In *Proceedings of the IEEE/CVF conference on computer vision and pattern recognition*, pages 8346–8355, 2020. 2
- [19] Diederik P Kingma and Jimmy Ba. Adam: A method for stochastic optimization. *arXiv preprint arXiv:1412.6980*, 2014. 7
- [20] Boyi Li, Felix Wu, Kilian Q Weinberger, and Serge Belongie. Positional normalization. *Advances in Neural Information Processing Systems*, 32, 2019. 5
- [21] Ruoteng Li, Loong-Fah Cheong, and Robby T Tan. Heavy rain image restoration: Integrating physics model and conditional adversarial learning. In *Proceedings of the IEEE/CVF conference on computer vision and pattern recognition*, pages 1633–1642, 2019. 6
- [22] Ruoteng Li, Loong-Fah Cheong, and Robby T Tan. Heavy rain image restoration: Integrating physics model and conditional adversarial learning. In *Proceedings of the IEEE/CVF conference on computer vision and pattern recognition*, pages 1633–1642, 2019. 2, 6
- [23] Ruoteng Li, Robby T Tan, and Loong-Fah Cheong. All in one bad weather removal using architectural search. In *Proceedings of the IEEE/CVF conference on computer vision and pattern recognition*, pages 3175–3185, 2020. 2, 3, 6, 7
- [24] Jiacheng Liu, Shenghua Teng, and Zuoyong Li. Removing rain from single image based on details preservation and background enhancement. In *2019 IEEE 2nd International Conference on Information Communication and Signal Processing (ICICSP)*, pages 322–326. IEEE, 2019. 1

- [25] Yun-Fu Liu, Da-Wei Jaw, Shih-Chia Huang, and Jenq-Neng Hwang. Desnownet: Context-aware deep network for snow removal. *IEEE Transactions on Image Processing*, 27(6): 3064–3073, 2018. 1, 2, 3, 6, 7
- [26] Jie Luo, Qirong Bu, Lei Zhang, and Jun Feng. Global feature fusion attention network for single image dehazing. In *2021 IEEE International Conference on Multimedia & Expo Workshops (ICMEW)*, pages 1–6. IEEE, 2021. 7
- [27] Ozan Özdenizci and Robert Legenstein. Restoring vision in adverse weather conditions with patch-based denoising diffusion models. *IEEE Transactions on Pattern Analysis and Machine Intelligence*, 2023. 2, 3
- [28] Rui Qian, Robby T Tan, Wenhan Yang, Jiajun Su, and Jiaying Liu. Attentive generative adversarial network for rain-drop removal from a single image. In *Proceedings of the IEEE conference on computer vision and pattern recognition*, pages 2482–2491, 2018. 2, 6
- [29] Yanyun Qu, Yizi Chen, Jingying Huang, and Yuan Xie. Enhanced pix2pix dehazing network. In *Proceedings of the IEEE/CVF conference on computer vision and pattern recognition*, pages 8160–8168, 2019. 2, 7
- [30] Ruijie Quan, Xin Yu, Yuanzhi Liang, and Yi Yang. Removing raindrops and rain streaks in one go. In *Proceedings of the IEEE/CVF Conference on Computer Vision and Pattern Recognition*, pages 9147–9156, 2021. 2, 6
- [31] Yuhui Quan, Shijie Deng, Yixin Chen, and Hui Ji. Deep learning for seeing through window with raindrops. In *Proceedings of the IEEE/CVF International Conference on Computer Vision*, pages 2463–2471, 2019. 2
- [32] Dongwei Ren, Wangmeng Zuo, Qinghua Hu, Pengfei Zhu, and Deyu Meng. Progressive image deraining networks: A better and simpler baseline. In *Proceedings of the IEEE/CVF conference on computer vision and pattern recognition*, pages 3937–3946, 2019. 7
- [33] Wenqi Ren, Si Liu, Hua Zhang, Jinshan Pan, Xiaochun Cao, and Ming-Hsuan Yang. Single image dehazing via multi-scale convolutional neural networks. In *Computer Vision—ECCV 2016: 14th European Conference, Amsterdam, The Netherlands, October 11–14, 2016, Proceedings, Part II 14*, pages 154–169. Springer, 2016. 1, 2
- [34] Jeya Maria Jose Valanarasu, Rajeev Yasarla, and Vishal M Patel. Transweather: Transformer-based restoration of images degraded by adverse weather conditions. In *Proceedings of the IEEE/CVF Conference on Computer Vision and Pattern Recognition*, pages 2353–2363, 2022. 2, 3, 6, 7, 4
- [35] Laurens Van der Maaten and Geoffrey Hinton. Visualizing data using t-sne. *Journal of machine learning research*, 9(11), 2008. 8, 3
- [36] Hong Wang, Qi Xie, Qian Zhao, and Deyu Meng. A model-driven deep neural network for single image rain removal. In *Proceedings of the IEEE/CVF conference on computer vision and pattern recognition*, pages 3103–3112, 2020. 2
- [37] Yinglong Wang, Chao Ma, and Bing Zeng. Multi-decoding deraining network and quasi-sparsity based training. In *Proceedings of the IEEE/CVF Conference on Computer Vision and Pattern Recognition*, pages 13375–13384, 2021. 1, 2
- [38] Zhou Wang, Alan C Bovik, Hamid R Sheikh, and Eero P Simoncelli. Image quality assessment: from error visibility to structural similarity. *IEEE TIP*, 13(4):600–612, 2004. 7
- [39] Haiyan Wu, Yanyun Qu, Shaohui Lin, Jian Zhou, Ruizhi Qiao, Zhizhong Zhang, Yuan Xie, and Lizhuang Ma. Contrastive learning for compact single image dehazing. In *Proceedings of the IEEE/CVF Conference on Computer Vision and Pattern Recognition*, pages 10551–10560, 2021. 7
- [40] Jie Xiao, Xueyang Fu, Aiping Liu, Feng Wu, and Zheng-Jun Zha. Image de-raining transformer. *IEEE Transactions on Pattern Analysis and Machine Intelligence*, 2022. 2
- [41] Dong Yang and Jian Sun. Proximal dehaze-net: A prior learning-based deep network for single image dehazing. In *Proceedings of the european conference on computer vision (ECCV)*, pages 702–717, 2018. 2
- [42] Wenhan Yang, Robby T Tan, Jiashi Feng, Jiaying Liu, Zongming Guo, and Shuicheng Yan. Deep joint rain detection and removal from a single image. In *Proceedings of the IEEE conference on computer vision and pattern recognition*, pages 1357–1366, 2017. 7
- [43] Wenhan Yang, Robby T Tan, Jiashi Feng, Zongming Guo, Shuicheng Yan, and Jiaying Liu. Joint rain detection and removal from a single image with contextualized deep networks. *IEEE transactions on pattern analysis and machine intelligence*, 42(6):1377–1393, 2019. 2
- [44] Xitong Yang, Zheng Xu, and Jiebo Luo. Towards perceptual image dehazing by physics-based disentanglement and adversarial training. In *Proceedings of the AAAI conference on artificial intelligence*, 2018. 2
- [45] Yuntong Ye, Yi Chang, Hanyu Zhou, and Luxin Yan. Closing the loop: Joint rain generation and removal via disentangled image translation. In *Proceedings of the IEEE/CVF conference on computer vision and pattern recognition*, pages 2053–2062, 2021. 7
- [46] Yuntong Ye, Changfeng Yu, Yi Chang, Lin Zhu, Xi-le Zhao, Luxin Yan, and Yonghong Tian. Unsupervised deraining: Where contrastive learning meets self-similarity. In *Proceedings of the IEEE/CVF Conference on Computer Vision and Pattern Recognition*, pages 5821–5830, 2022. 2
- [47] Syed Waqas Zamir, Aditya Arora, Salman Khan, Munawar Hayat, Fahad Shahbaz Khan, Ming-Hsuan Yang, and Ling Shao. Multi-stage progressive image restoration. In *Proceedings of the IEEE/CVF conference on computer vision and pattern recognition*, pages 14821–14831, 2021. 6, 7
- [48] He Zhang, Vishwanath Sindagi, and Vishal M Patel. Image de-raining using a conditional generative adversarial network. *IEEE transactions on circuits and systems for video technology*, 30(11):3943–3956, 2019. 2
- [49] Kaihao Zhang, Dongxu Li, Wenhan Luo, and Wenqi Ren. Dual attention-in-attention model for joint rain streak and raindrop removal. *IEEE Transactions on Image Processing*, 30:7608–7619, 2021. 2
- [50] Kaihao Zhang, Rongqing Li, Yanjiang Yu, Wenhan Luo, and Changsheng Li. Deep dense multi-scale network for snow removal using semantic and depth priors. *IEEE Transactions on Image Processing*, 30:7419–7431, 2021. 2, 6
- [51] Zheyu Zhang, Yurui Zhu, Xueyang Fu, Zhiwei Xiong, Zheng-Jun Zha, and Feng Wu. Multifocal attention-based

- cross-scale network for image de-raining. In *Proceedings of the 29th ACM International Conference on Multimedia*, pages 3673–3681, 2021. 2
- [52] Lei Zhu, Chi-Wing Fu, Dani Lischinski, and Pheng-Ann Heng. Joint bi-layer optimization for single-image rain streak removal. In *Proceedings of the IEEE international conference on computer vision*, pages 2526–2534, 2017. 1
- [53] Lei Zhu, Zijun Deng, Xiaowei Hu, Haoran Xie, Xuemiao Xu, Jing Qin, and Pheng-Ann Heng. Learning gated non-local residual for single-image rain streak removal. *IEEE Transactions on Circuits and Systems for Video Technology*, 31(6):2147–2159, 2020. 2
- [54] Yurui Zhu, Tianyu Wang, Xueyang Fu, Xuanyu Yang, Xin Guo, Jifeng Dai, Yu Qiao, and Xiaowei Hu. Learning weather-general and weather-specific features for image restoration under multiple adverse weather conditions. In *Proceedings of the IEEE/CVF Conference on Computer Vision and Pattern Recognition*, pages 21747–21758, 2023. 2, 3, 6, 7, 4

Decoupling Degradation and Content Processing for Adverse Weather Image Restoration

Supplementary Material

6. Channel Statistics

In the main text, Fig. 2 warrants further explanation, which we provide here. Specifically, we delve deeper into the visualization of features, conducting a thorough examination of how different types of degradation manifest themselves as unique variations in the distribution of channels. This analysis not only illustrates the impact of degradation but also the nuances of its effects across various layers of the network. Furthermore, we explore the role of the mean operation across channel dimensions in detail, emphasizing its effectiveness in diminishing the influence of degraded information. This process plays a crucial role in refining the quality of the content extracted from these images.

We have visualized images of various adverse weather conditions through the intermediate features and gradients at each feature layer within the network, as shown in Fig. 9, Fig. 10 and Fig. 11. This visualization process allows us to closely examine the intricate details and transformations that these images undergo during their progression through the network. By focusing on both the intermediate features and their corresponding gradients, we gain a comprehensive understanding of how different types of image degradation are processed and altered at each layer of the network.

We input 500 images each of rain, haze, and snow into the network, and visualized the t-SNE clustering of their intermediate features. As shown in Fig. 13, for instance, the left side illustrates how features are primarily clustered by the type of degradation before the mean operation across the channel dimension. However, on the right side, post-mean operation, the degradation information is markedly lessened. This reduction allows for a more content-centric clustering of features, highlighting the mean operation’s ability to enhance the network’s focus on the essential aspects of the images, irrespective of the degradation type.

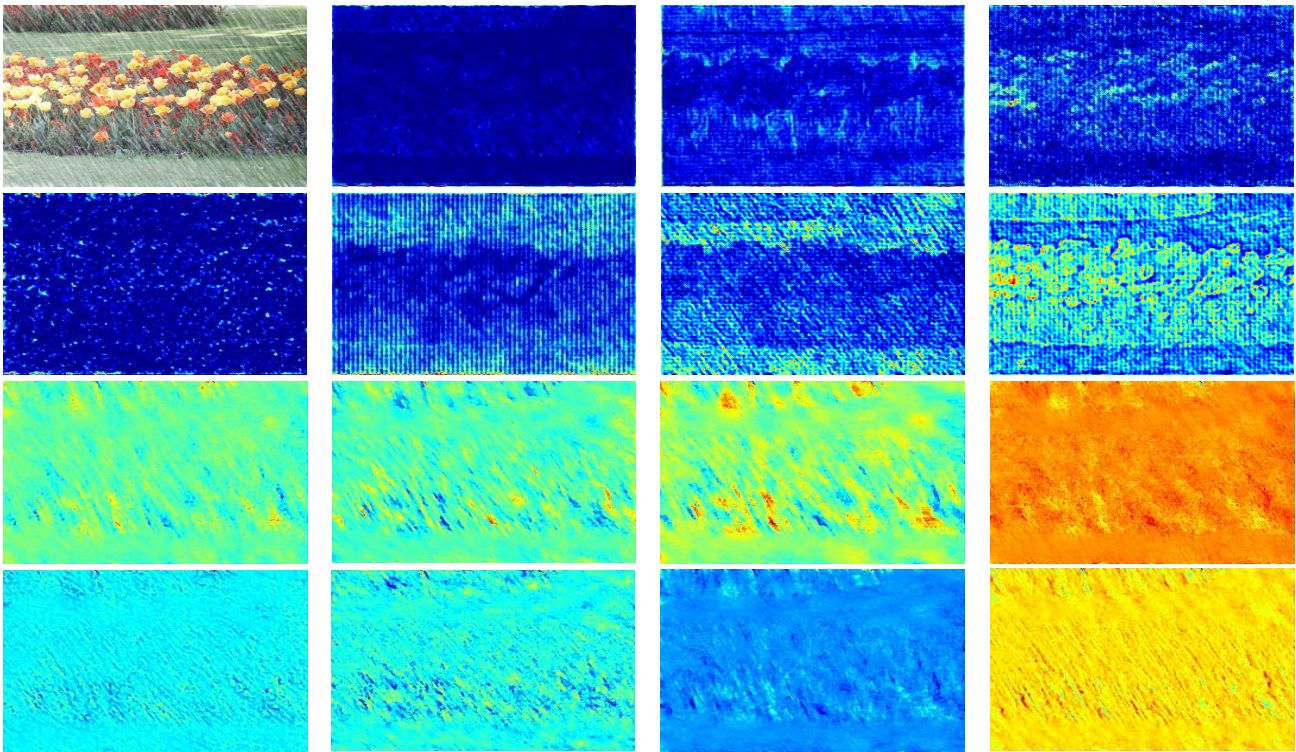


Figure 9. Visualization of the intermediate features of **rain** images within the network (top two rows), and the corresponding gradients of the intermediate features (bottom two rows).

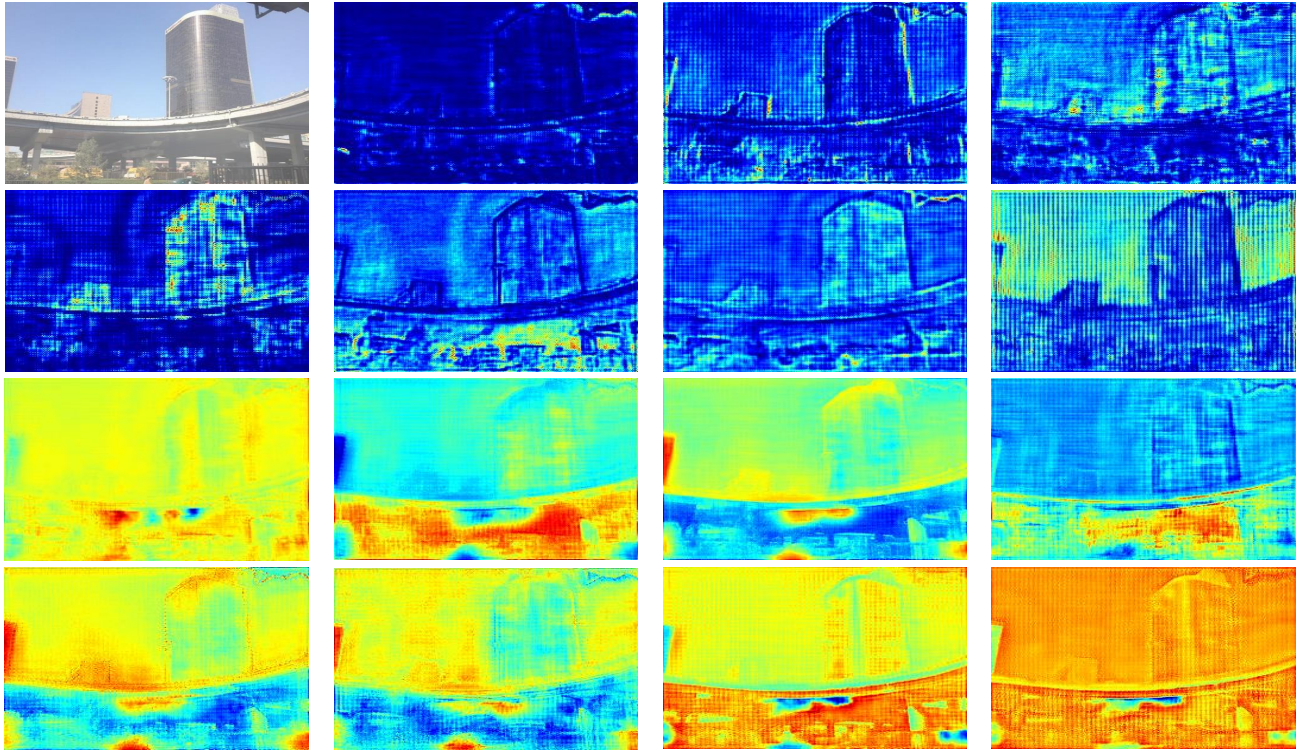


Figure 10. Visualization of the intermediate features of **haze** images within the network (top two rows), and the corresponding gradients of the intermediate features (bottom two rows).

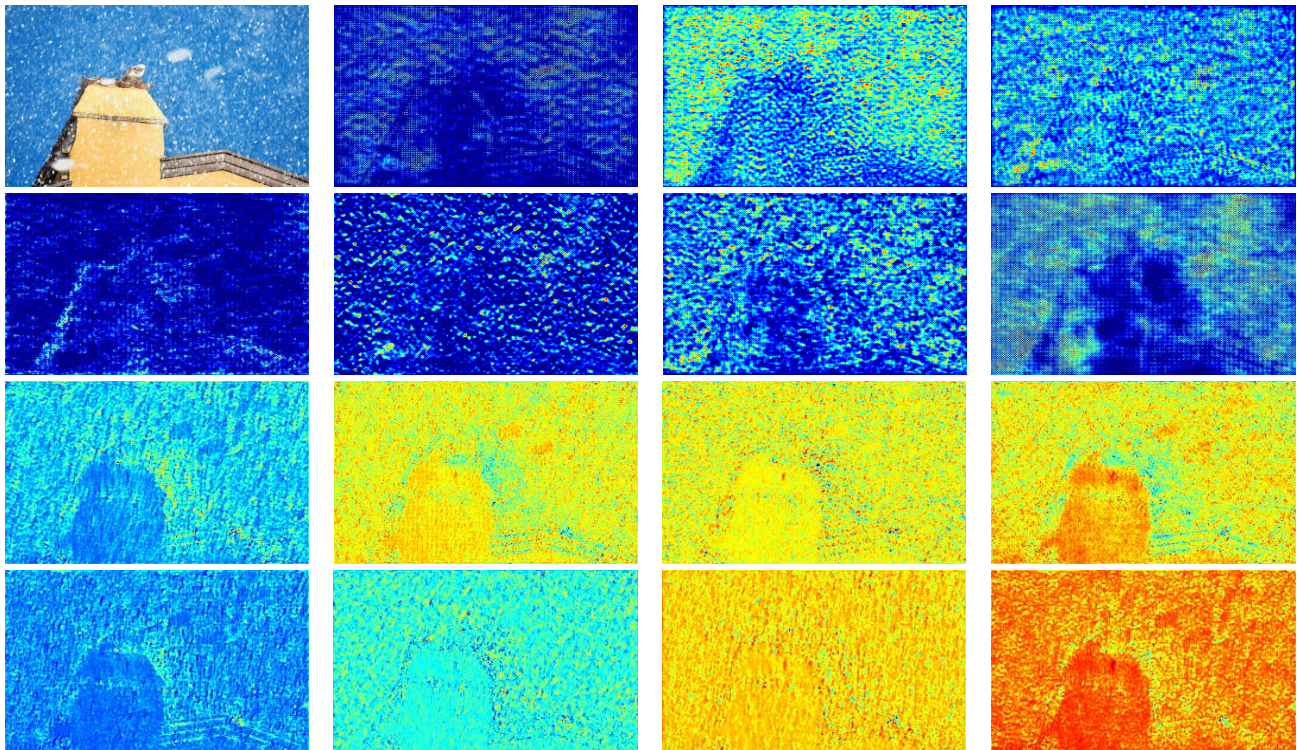


Figure 11. Visualization of the intermediate features of **snow** images within the network (top two rows), and the corresponding gradients of the intermediate features (bottom two rows).

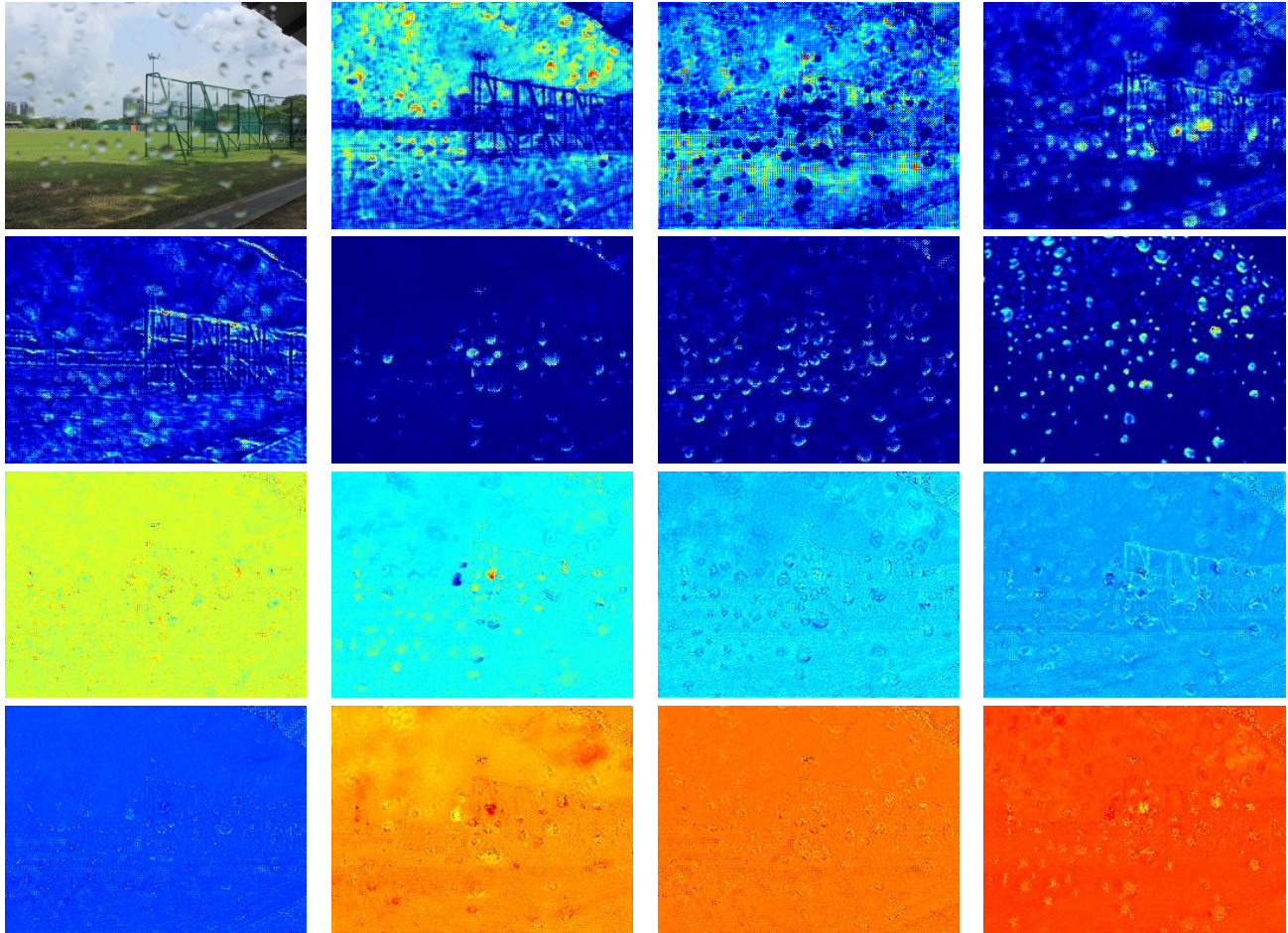


Figure 12. Visualization of the intermediate features of **raindrop** images within the network (top two rows), and the corresponding gradients of the intermediate features (bottom two rows).

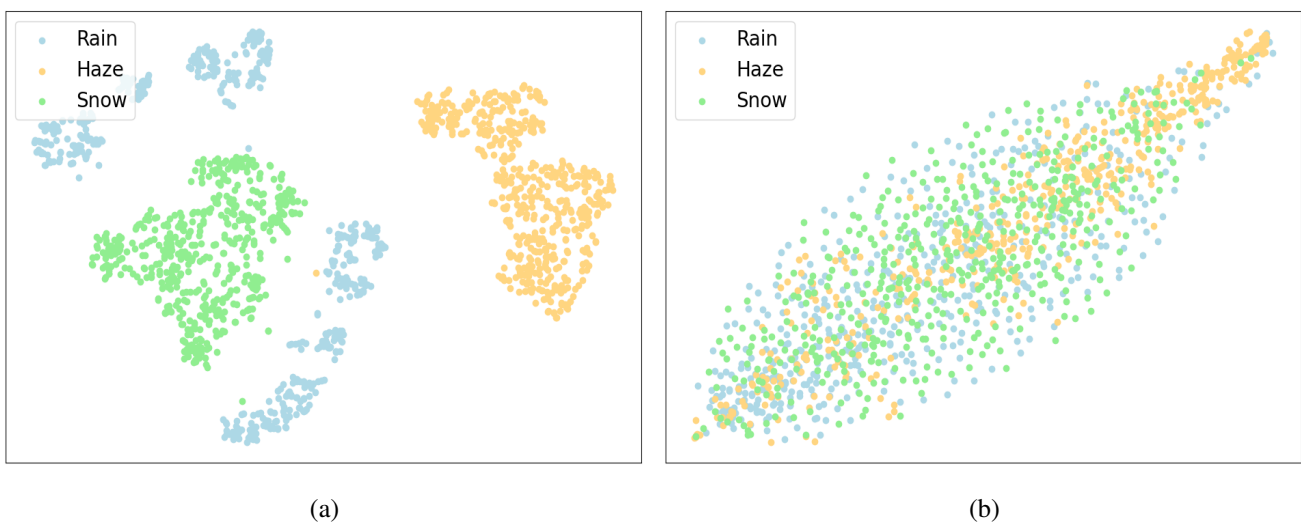


Figure 13. The t-SNE [35] visualization of the intermediate features, (a): before the mean operation across the channel dimension, (b): after the mean operation across the channel dimension.



Input Chen *et al.* [4] TransWeather [34] Zhu *et al.* [54] Ours

Figure 14. Visual comparison of image desnowing on the realistic dataset. Zoom in for better comparison.

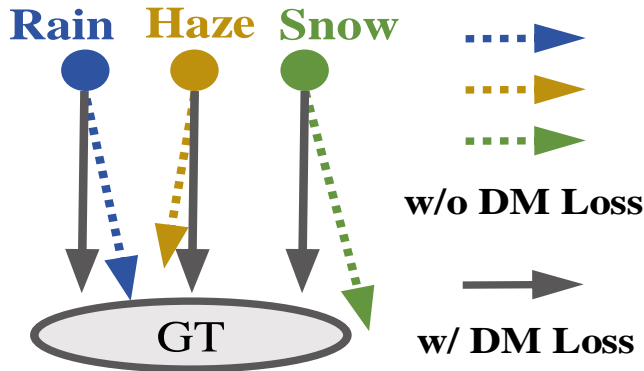


Figure 15. The effect of the degradation mapping loss.

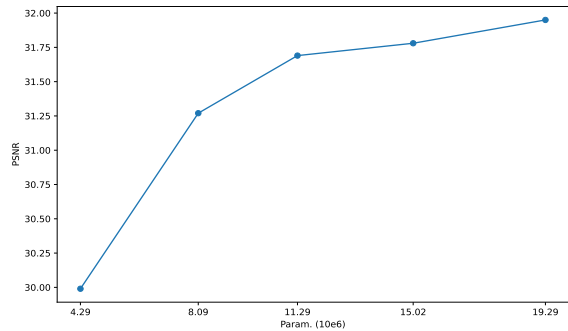


Figure 16. Quantitative analysis of the network's performance under different parameter numbers.

7. Experiments

Snow visualization. Due to space limitations in the main text, we did not show the visual effect images of snow scenes. Here, we present a set of comparative visual effect images of snow scenes in Fig. 14. It can be seen that the images output by our network have better clarity and color contrast.

Degradation Mapping Loss. We further provide a schematic illustration of the Degradation Mapping Loss constraint in Fig. 15. It can be observed that without this loss, the optimization directions for different weather conditions vary. However, with the incorporation of this loss, the optimization directions for various weather conditions become consistent.

Ablation study of the parameter numbers. We conduct a quantitative analysis on the test set of the Rain1400 dataset to evaluate the impact of different parameter quantities on network performance as shown in Fig. 16. It can be observed that with a smaller number of parameters, an increase in parameters leads to a significant improvement in performance. However, with a larger number of parameters, the enhancement in performance due to an increase in parameters is limited.